$(\sqrt{3}\times\sqrt{3})R30°$-(K+CO) coadsorption structure on Pt(111): Experiment and theory

S. Moré*
Fritz-Haber-Institut der Max-Planck-Gesellschaft, Faradayweg 4-6, D-14195 Berlin, Germany

Ari P Seitsonen†
Fritz-Haber-Institut der Max-Planck-Gesellschaft, Faradayweg 4-6, D-14195 Berlin, Germany;
Istituto Nazionale di Fisica della Materia, Unità di Roma, Università La Sapienza, P.le. A. Moro 2, 00185 Roma, Italy;
and Max-Planck-Institut für Plasmaphysik, Boltzmannstrasse 2, D-85748 Garching bei München, Germany

W. Berndt
Fritz-Haber-Institut der Max-Planck-Gesellschaft, Faradayweg 4-6, D-14195 Berlin, Germany

A. M. Bradshaw
Max-Planck-Institut für Plasmaphysik, Boltzmannstrasse 2, D-85748 Garching bei München, Germany
(Received 30 November 2001; revised manuscript received 13 May 2002; published 29 October 2002)

We report joint experimental and theoretical investigations of the $(\sqrt{3}\times\sqrt{3})R30°$-(K+CO) coadsorption phase on Pt(111). The studies were performed with low-energy electron diffraction structural analysis and density functional theory calculations based on the generalized gradient approximation. The measured and calculated adsorption geometries agree quantitatively. Both CO and K are found to occupy threefold symmetric hcp hollow sites. The internal C-O bond elongates upon the coadsorption of K with respect to the pure CO/Pt(111) phase, and likewise the K-surface separation increases with respect to the $(\sqrt{3}\times\sqrt{3})R30°$-K phase on Pt(111).

DOI: 10.1103/PhysRevB.66.165424 PACS number(s): 68.35.Bs

I. INTRODUCTION

Alkali metals act as promoters in various catalytic reactions.[1] The adsorption of alkali metals on transition metal surfaces has therefore been investigated for a large number of systems; studies of their coadsorption with reactants, intermediates, and reaction products can also yield important insight into chemical reactivity and catalysis. Coadsorption of alkali metals with CO gives rise to model systems of high complexity which are closely related to the microscopic processes occurring in heterogeneous catalysts of industrial applicability, although the detailed structure of the latter is certainly more complicated. These systems have consequently attracted considerable interest in recent years, in particular K+CO on Pt(111).[2] The chemisorption properties of CO are drastically changed upon alkali metal adsorption: an increased heat of adsorption, shifts in the electron binding energies of the core and valence levels and, usually, a decrease in the C-O stretching frequency. For reviews of previous studies as well as a discussion of their findings the reader is referred to the articles by Bonzel[3] and Heskett.[4] An extensive overview of alkali metal adsorption and CO-alkali metal coadsorption, in particular the structural aspects, has been recently presented by Diehl and McGrath.[5]

In the past the most detailed qualitative studies concerning coadsorption of K+CO/Pt(111) and related systems have been carried out using vibrational spectroscopic methods as high resolutaion electron energy loss spectroscopy (HREELS) and infrared adsorption spectroscopy (IRAS).[6,7] These investigations have found as a general trend a softening of the internal C-O vibration, thus a weakening of the C-O bond due to the coadsorption of the alkali metal. However, only a few coadsorption systems have been studied in greater detail. Moreover, there are few quantitative structure analyses. Only five systems have been solved so far:[8] Ru(0001)-(2×2)-(K+CO),[9] Ru(0001)-(2×2)-(Cs+CO),[10] Ru(0001)-(2×2)-(Cs+2CO),[10] Co(10$\bar{1}$0)-(2×2)-(K+CO),[12] and Ni(111)-(2×2)-(K+CO).[11] The first two exhibit a substantial lengthening of the C-O bond; in the others the experimental error bars do not allow a definitive conclusion. Another open question concerns the influence of the CO on the bondlength of the alkali atom to the substrate.

A further motive for the study of an alkali-CO coadsorption system is the interest in pure alkali metal surface structures. It was demonstrated on aluminum that several alkali metals occupy on-top or substitutional sites with only a minor energy difference.[13] In recent studies we have estimated the energy difference between the hcp and fcc threefold hollow adsorption sites of K on Pt(111) to be 15 meV (Ref. 14) using the local density approximation and 10 meV (Ref. 15) employing the generalized gradient approximation in density functional calculations. The hcp site is favored, which was confirmed exclusively by the dynamical LEED analysis. The presence of a coadsorbate could, however, influence the energetic balance between these sites.

The phase diagram of coadsorbed K and CO on Pt(111) has been characterized using LEED and TDS and exhibits a variety of structures.[16] The observed increase in the desorption temperature implies either a strengthening of the CO-substrate bond or a mutually attractive K-CO interaction. The decrease of the work function caused by K on Pt(111) is reversed when CO is coadsorbed.[17] Angle resolved x-ray photoemission spectroscopy (XPS) has indicated that the

C-O molecular axis is oriented perpendicular to the substrate surface and that the molecule binds via the carbon atom to the Pt substrate.[18] However, no quantitative structural analysis has been carried out, although it was the experimental work of Somerjai[2] and Bonzel[3] on this system which initiated the great interest in alkali-metal/CO coadsorption systems. Cluster calculations have favored either a hollow site for the CO[19] or suggested a bridge site,[20] while for the alkali metal adsorbate a hollow site has been proposed.[19]

We present a dynamical LEED structural analysis of the $(\sqrt{3}\times\sqrt{3})R30°$-(K+CO) phase on Pt(111) at coverages $\Theta = 0.33$ for both K and CO. The results are compared to density functional-based first principles calculations.

II. SAMPLE PREPARATION AND LEED MEASUREMENT

A $5N$ Pt crystal of dimensions 8 mm×8 mm×2 mm was oriented to within 0.5° of the [111] orientation. The temperature was measured using a Ni/NiCr thermocouple and could be varied via resistive heating between 90 and 1400 K using a programmable power control unit. To clean the surface several cycles of argon ion bombardment and annealing to 800 K were required. Auger measurements show that carbon was the main contaminant. Using the cleaning cycle contamination could be reduced until the ratio between the Auger amplitudes from carbon at 272 eV and platinum at 64 eV was 4×10^{-4}. K was deposited from a commercial SAES getter source (SAES Getters SpA) with the crystal held at 100 K. The source was thoroughly out gassed prior to each experiment. Adsorption at room temperature or adsorption at 100 K and subsequent annealing at 270 K did not change the measured $I(V)$ curves substantially.

Two different approaches were applied to obtain the $(\sqrt{3}\times\sqrt{3})R30°$-(K+CO) overlayer: In the first case a $(\sqrt{3}\times\sqrt{3})R30°$-K overlayer was deposited and subsequently CO was dosed until the additional LEED spots reached maximum intensity. In the second approach CO was adsorbed until a $c(2\times4)$ pattern was reached, implying a CO coverage of $\Theta=0.5$,[21] and thereafter K was deposited. This procedure resulted in the formation of a (3×3) diffraction pattern, which was unstable under the electron bombardment during the LEED measurement and transformed reversibly into a $(\sqrt{3}\times\sqrt{3})R30°$ structure. Its $I(V)$ curves were identical with those of the first method of preparation. On reduction of the electron beam current the (3×3) structure slowly reappeared.

All experiments were carried out at background pressures below 10^{-10} mbar. The LEED intensities at 100 K sample temperature were measured using a Varian three-grid optics and a video-LEED system (AIDA) from Vacuum Science Instruments. The LEED patterns from the clean surface as well as from the overlayer structures were characterized by sharp spots and a low background intensity. The energy of the electron beam was varied in steps of 1 eV from 40–50 eV to 400 eV. Three sets of $I(V)$ curves were taken for the $(\sqrt{3}\times\sqrt{3})R30°$-(K+CO) overlayer at three different angles of incidence and were compared to dynamical LEED calculations. Two data sets were measured with preadsorbed K, one with preadsorbed CO. The clean surface was also checked and the results compared with those in our previous paper.[14]

III. THE LEED-I(V) ANALYSIS

A. Calculation

The LEED results were analyzed using a fully dynamical multiple scattering code developed by Moritz.[22] The program uses the layer KKR and the ''layer-doubling'' method.[23] For the Pt, C, and O atomic potential phase shifts up to $l=10$ derived from self-consistent band structure calculations were used. For K the potential from the literature[24] was taken. To determine the adsorption structure a grid search was performed, which included adsorption sites and the first two layer distances. The following high symmetry adsorption geometries were considered in the analysis: the threefold-hollow sites (hcp and fcc), the bridge site and the on-top site. A structure with K in a substitutional surface site was also investigated. From Fig. 1 it is evident that some of these combinations exhibit a strong steric hindrance, especially if the C-O axis were to remain perpendicular to the substrate surface. The substitutional site leads to a large separation between K and Pt atoms. The agreement between the calculated and measured $I(V)$ curves was quantified by the R_P (Ref. 25) and R_{DE} (Ref. 26) reliability factors. The hcp hollow site geometries for both K and CO resulted in the lowest r factors. The hcp and fcc as well as bridge (CO) and hollow site (K) were further refined, based on minimizing R_P, by considering a translational shift of the K and CO towards each other. We subsequently optimized the Debye temperatures and simulated the vibrational motion of the K using the method of split positions.[27] Figure 1 provides an overview of the investigated structures, and the r-factors are listed in Table I.

In LEED analysis the surface vibrations are usually accounted for by a variation of the surface Debye temperature (and to a lesser extent by adjusting the imaginary part of the inner potential). The Debye temperature T_D, however, only accounts for isotropic vibrations, whereas adatoms on surfaces vibrate anisotropically. It is possible to determine the anisotropic vibrational amplitudes with the split position approach.[27] We have used this method, replacing the K atom by three equivalent atoms of weight 1/3, each laterally displaced by r_{split} from the mean position. Multiple scattering between these split atoms is suppressed and the Debye temperature is refined along with the split positions. The apparent Debye temperature is increased when the split positions method is invoked in the analysis because the latter already partially accounts for vibrations parallel to the surface. The final average of the r factors for the best fit structure was 0.32 (R_P). The r factors for the three data sets were 0.315 (normal incidence), and 0.34 and 0.32 for the off-angle data set for K, respectively, CO precoverage. Figure 2 shows the best-fit $I(V)$ curves obtained from the LEED analysis for the K precovered surface.

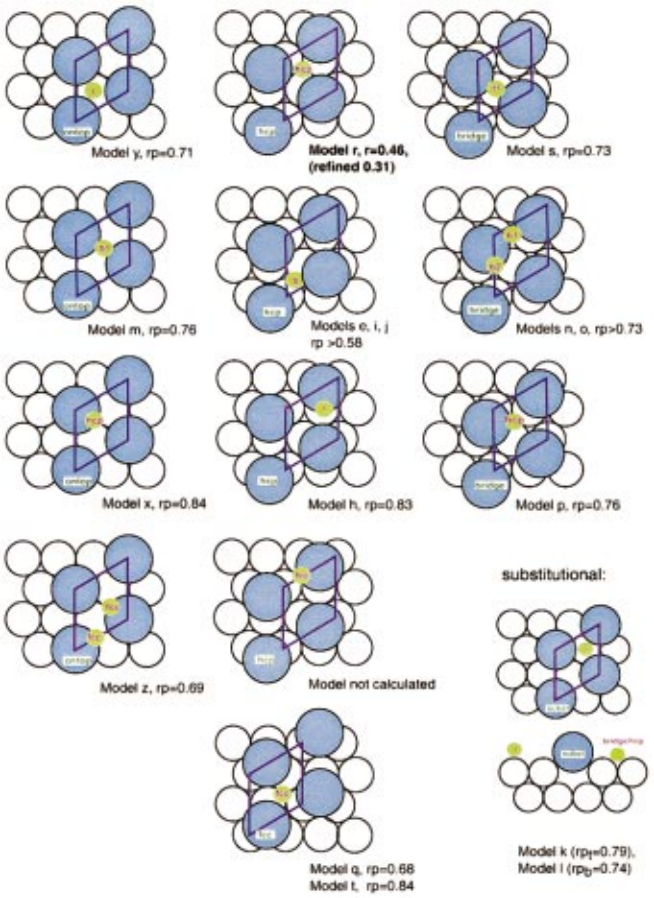

FIG. 1. (Color) Models investigated for the $(\sqrt{3}\times\sqrt{3})R30°$-(K+CO) on Pt(111); gray symbols represent K, yellow symbols CO. The fcc site, which differs from the hcp only by the Pt-substrate stacking order, is depicted only for the fcc/fcc combination. The *r* factors are for the normal incidence data set.

B. Geometry from the LEED analysis

The best fit structure obtained from the LEED analysis consisted of CO and K in hcp hollow sites corresponding to model *r* in Fig. 1, and is depicted in more detail in Fig. 3. In this arrangement both K and CO are mutually threefold coordinated. The bondlength between the K and the three nearest neighbor platinum surface atoms is 3.28 ± 0.04 Å, the distance between C and Pt 2.08 Å, and the C-O bondlength 1.26 Å. The average first Pt interlayer spacing is expanded by 0.7% compared to the bulk. This is slightly smaller than the expansion measured for the clean surface, which is about 1%. No expansion or contraction is detectable in the deeper layers. $(\sqrt{3}\times\sqrt{3})R30°$ phases of alkali metals in threefold symmetric hollow sites have been observed for K, Rb, and Cs on Rh(111),[27] Ru(0001),[28] Ag(111),[29] and for K (Ref. 14) and Na (Refs. 30,15) on Pt(111). The use of split positions reduces R_P by about 10%. The calculated in- and out-of-plane vibrational amplitudes and the isotropic Debye temperatures T_D are listed in Table II. These values are similar to the value found for K on Pt(111) without coadsorbed CO.[14] An anisotropic variation of the K position showed that a shift of 50% of the K towards the CO along with a larger lateral vibration simulated by split positions did not result in a higher *r* factor. The improvement in the value was, however, very small, and the corresponding error bars large. Such a structure would correspond to a disordered $(3\times\sqrt{3})$ unit cell. This structure would also lead to the same LEED pattern as that obtained from a $(\sqrt{3}\times\sqrt{3})R30°$ structure. The improvement in the *r*-factor values was, however, very small. A partial site occupancy of either K or CO on a non-hcp site could be safely excluded on the basis of the *r* factors (see Table I).

C. CO coverage

The K/CO $(\sqrt{3}\times\sqrt{3})R30°$ structure, which has been solved using LEED in this paper, forms (see also Sec. II) either after preadsorption of 0.33 ML potassium and subsequent CO adsorption or after 0.5 ML CO adsorption and subsequent K deposition. The main difference between these two preparation methods is that CO precoverage leads first to the formation of a (3×3) unit cell, which only gradually, over a period of 15 min, rearranges into the $(\sqrt{3}\times\sqrt{3})R30°$ unit cell. For the CO precoverage this phase transition is reversible and the pattern only stable under electron bombardment. This contrasts with the stable $(\sqrt{3}\times\sqrt{3})R30°$ structure formed if K is deposited first. Both variants, however, lead to practically identical LEED $I(V)$ curves and consequently to the same geometrical structure. As the coverage of both K and CO is 0.33 ML in our best fit model, the missing CO has to be accounted for in the case of CO preadsorption. A K:CO ratio of less than 1:1.5 would correspond to the initial coverage of $\Theta=0.5$ of the preadsorbed $c(2\times4)$-CO phase (Fig. 4). The most likely explanation is a partial desorption of the CO during K deposition, so that a variable CO concentration could result in the CO-adsorbed phase. We have therefore examined the influence of the CO coverage on the *r* factor. K:CO ratios of 1:0.5, 1:1.25, 1:1.5, 1:2 were simulated in the LEED analysis for the CO precovered surface (Table III). The *r* factors exclude ratios higher than 1:1.25 and in fact a slight CO deficiency (i.e., less than 1:1) is in better agreement with the *r* factors for off-normal incidence. Since the metastable (3×3) phase was not investigated in this study, its K and CO sites are as yet undetermined. A possible arrangement is shown in Fig. 4, depicting both K and CO on the threefold symmetric hcp sites. The formation of the (3×3) is a clear indication of a medium to long range interaction between the adsorbate adatoms beyond the nearest neighbors.

IV. DENSITY FUNCTIONAL CALCULATIONS

A. Calculational details

The density functional calculations were performed using the generalized gradient approximation (GGA) of Perdew *et al.*[31] as the exchange-correlation term in the Kohn-Sham formalism. The orbitals were expanded using a plane wave basis up to a cutoff energy of 50 Ry, and those for the plane waves for a density up to a cutoff of 190 Ry. Pseudopotentials were used to remove the sharp features of the valence orbitals in the core region and to model the influence of the

TABLE I. r factors of models investigated in the LEED calculations. The coordinates are given in fractions of the $(\sqrt{3}\times\sqrt{3})R30°$ superstructure cell. The angle between the ordinates is 60°.

	$\theta=-5°$, $\theta=14°$ normal incidence						
Model	R_{DE}	R_P	R_{DE}	R_P	Comment	K coordinates	CO coordinates
a	0.54	0.67	0.55	0.89	K fcc, no CO	0.333, 0.000	
b	0.57	0.78	0.51	0.77	K hcp, no CO	−0.333, 0.000	
c	0.57	0.85	0.64	0.84	K on-top, no CO	0.000, 0.000	
d	0.55	0.87	0.59	0.83	K bridge, no CO	0.000, 0.500	—
e	0.57	0.85	0.64	0.58	K hcp, 1 CO bridge	−0.333, 0.000	0.000, 0.500
f	0.70	0.75	0.73	0.68	K hcp, 2 CO bridge	−0.333, 0.000	0.667 0.667; 0.167, 0.333
g	0.69	0.73	0.73	0.94	K fcc, 1 CO bridge	0.333, 0.000	0.167, 0.500
h	0.74	0.78	0.75	0.83	K hcp, 1 CO on-top	−0.333, 0.000	0.000, 0.000
i	0.82	0.88	0.53	0.73	K hcp, 2 CO bridge	−0.333, 0.000	0.333, 0.500; −0.167, 0.500
j	0.82	0.87	0.63	0.77	K hcp, 2 CO bridge	−0.333, 0.000	0.500, 0.167; −0.167, −0.167
k	0.67	0.86	0.59	0.79	K substitutional, 1 CO on-top	0.000, 0.000, −1.00	0.333, 0.333
l	0.64	0.80	0.57	0.74	K substitutional, 1 CO bridge	0.000, 0.000, −1.00	0.500, 0.500
m	0.67	0.80	0.55	0.76	K on-top, 1 CO bridge	0.000, 0.000	0.500, 0.500
n	0.83	0.88	0.57	0.74	K bridge, 1 CO bridge	−0.167, −0.167	0.500, 0.500
o	0.78	0.87	0.55	0.69	K bridge, 1 CO bridge	−0.167, −0.167	0.500, 0.000
p	0.75	0.86	0.64	0.76	K bridge, 1 CO hcp	−0.167, −0.167	0.000, 0.333
q	0.68	0.76	0.68	0.75	K fcc, 1 CO fcc	0.333, 0.000	0.667, 0.333
r	**0.47**	**0.58**	**0.36**	**0.46**	K hcp, CO hcp	0.333, 0.000	0.667, 0.667
r	**0.32** for the refined model						
s	0.82	0.88	0.53	0.73	K bridge, CO (t1) on-top	−0.167, −0.167	0.333, 0.333
t	0.69	0.78	0.64	0.84	K fcc, 2 CO fcc	0.333, 0.000	0.667, 0.333; 0.000, 0.667
u	0.58	0.81	0.51	0.61	K, CO hcp, disordered		
v	0.54	0.77	0.56	0.79	K, CO bridge, disordered		
w	0.52	0.67	0.54	0.84	K, CO fcc, disordered		
x	0.81	0.81	0.58	0.67	K on-top, 1 CO fcc	0.000, 0.000	0.333, 0.000
y	0.67	0.75	0.67	0.71	K on-top, 1 CO on-top	0.000, 0.000, 0.333, 0.333	
z	0.64	0.72	0.55	0.69	K on-top, 1 CO hcp	0.000, 0.000	−0.333, 0.000
N1	0.45	0.68	0.43	0.51	K hcp, CO bridge		
N2	0.61	0.74	0.56	0.67	K bridge, CO hcp		
N3	0.64	0.88	0.61	0.72	K fcc, CO bridge		
N4	0.71	0.82	0.59	0.76	K bridge, CO fcc		

core electrons on the valence electrons.[32] The adsorption geometry consisted of a slab of five Pt layers separated by the equivalent of 16 Å of vacuum to isolate the slabs. The adatoms were placed only on one side of the slab and the dipole correction[33] balanced the different asymptotic electrostatic potentials at the two sides. The two upper-most substrate layers were allowed to relax. Four k points were used in the irreducible wedge of the Brillouin zone of the $(\sqrt{3}\times\sqrt{3})R30°$ supercell to approximate the integrals over the first Brillouin zone, and they were generated using the generalized Cunningham point scheme.[34] The integration was stabilized with a Fermi function with a width of 0.1 eV. The resulting lattice constant of bulk platinum was 4.021 Å, about 2.5% larger than the experimental value of 3.92 Å. Such an overestimation is typical for the generalized gradient approximation.

The electronic structure of the adsorbed system was analyzed using the projected density of states $\mathcal{P}$ (PDOS) for Pt and K, and the orbital overlap $\mathcal{O}$ for CO. The PDOS as a function of energy E for an atomic orbital $\phi_{I,lm}(\mathbf{r}-\mathbf{R}_I)$ with the angular momentum l,m around an atom I at $\mathbf{R}_I$ is defined as

$$\mathcal{P}_{I,lm}(E)=\sum_{i,\mathbf{k}} \omega_{\mathbf{k}} f_{i,\mathbf{k}} |\langle \phi_{I,lm}|\psi_{i,\mathbf{k}}\rangle|^2 \delta(E-E_{i,\mathbf{k}}), \quad (1)$$

where $\psi_{i,\mathbf{k}}$ are the Kohn-Sham states i at point $\mathbf{k}$ in the first Brillouin zone of the adsorption system, $\omega_{\mathbf{k}}$ and $f_{i,\mathbf{k}}$ are the corresponding weights and occupation numbers, and $E_{i,\mathbf{k}}$ are the Kohn-Sham energy eigenvalues. $\delta(E)$ is in principle Dirac's delta function. However, due to the finite number of states in our calculation we replace the delta function with Gaussian broadening around the eigenvalues $E_{i,\mathbf{k}}$. The atomic radial functions are cut off at a certain radius somewhat below the interatomic distance in order to avoid overcounting of the overlap with distant atoms.

The orbital overlap is defined in the similar manner, however, instead of the atomic orbitals the states of the adsorbate

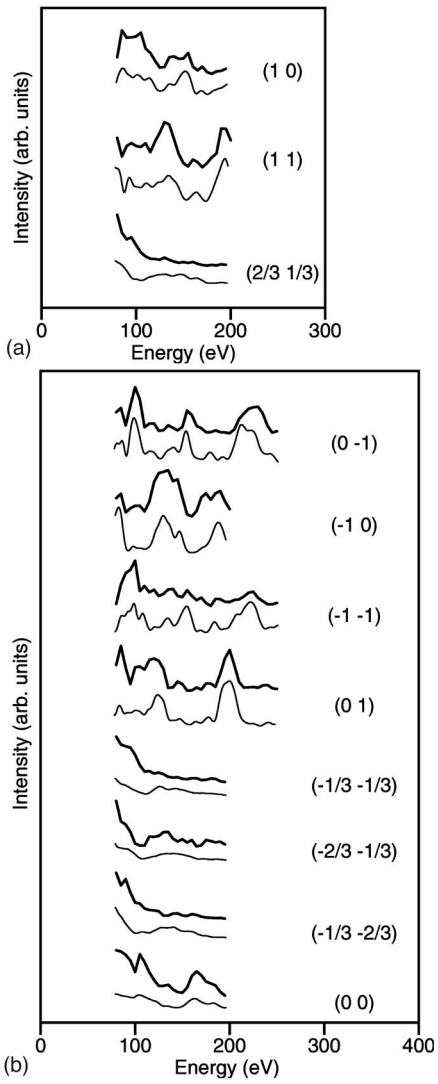

FIG. 2. LEED $I(V)$ curves for (a) normal and (b) off-normal incidence for K and CO at hcp hollow sites; $R_P = 0.32$ and 0.34, respectively.

system are projected on the molecular states χ_j of the carbon monoxide, always positioned in the same geometry as in the adsorbate system

$$\mathcal{O}_j(E) = \sum_{i,\mathbf{k}} \omega_{\mathbf{k}} f_{i,\mathbf{k}} |\langle \chi_j | \psi_{i,\mathbf{k}} \rangle|^2 \times \delta(E - E_{i,\mathbf{k}}); \qquad (2)$$

j is the index for the molecular states.

Thus the PDOS and orbital overlap measure the contribution or ''weight'' of the respective adsorbate states in the adsorbed states, and are energy resolved. An detailed discussion of that approach is given, e.g., in Ref. 35. For example in Fig. 5(a) the *d* bands of the Pt atom in the surface layer of clean Pt(111) are seen, and the molecular states of CO in Fig. 5(c). The accuracy of the energy levels is approximately 0.5 eV, increasing to 1.0 eV towards the Fermi level. The energy scale is derived from the Kohn-Sham eigenvalues. The Kohn-Sham eigenvalues and thus the energy scale is not very accurate because of the approximations of the exchange-correlation functional used. There is no proof for a physical meaning ''per se'' of the Kohn-Sham eigenvalues (beyond the highest occupied one), but we are interested the qualitative effects and trends, and these come out quite accurately.

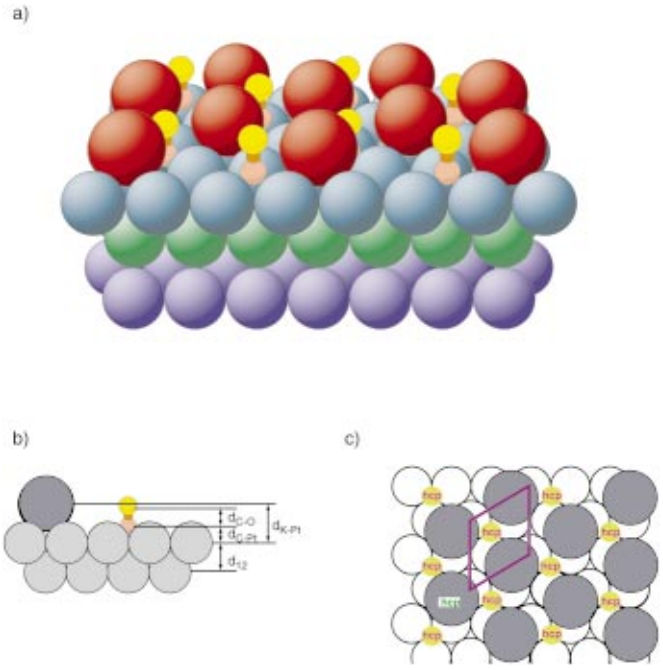

FIG. 3. (Color) Model of the on Pt(111)-$(\sqrt{3}\times\sqrt{3})R30°$-(K+CO) best-fit structure. (a) Perspective view, (b) side view, (c) top view. K atoms are depicted as large red, respective larger black circles, CO molecules yellow (gray), and respective partially filled circles.

B. Geometry of the K+CO-coadsorption structure on Pt(111) surface from DFT-GGA calculations

The adsorption of K and CO at hcp sites was investigated with DFT-GGA calculations. Results for other adsorption geometries will be reported elsewhere.[36] In the $(\sqrt{3}\times\sqrt{3})R30°$-(K+CO) structure the K atoms are separated from their Pt neighbors by 3.26 Å. The C-O bondlength is 1.27 Å and the Pt-C bondlength 2.08 Å. These numbers are very close to the LEED result. The first Pt interlayer expansion is +4.5%, while experimentally this value is only +0.7%. A similar overestimation for the first substrate layer spacing thus occurs for the K/Pt(111) structure when treated with GGA with the same methodology, but the same K-Pt distance are obtained as in the LEED result. We therefore assume that this overestimation does not interfere with the calculation of the the Pt-C, C-O, and K-Pt bondlengths in the coadsorbate structure.

V. DISCUSSION

The LEED structure analysis presented in this paper shows that both CO and K in the $(\sqrt{3}\times\sqrt{3})R30°$-(K+CO) on Pt(111) occupy hcp hollow sites. The LEED analysis therefore confirms recent cluster calculations, which propose the lowest energy for hollow sites for K on Pt(111).[19]

TABLE II. Structural parameters of the best fit model, i.e., the hcp site, from the LEED analysis together with the geometry parameters from the DFT-GGA calculations. Values given in percent relative to differences from the respective pure Pt(111)-($\sqrt{3}\times\sqrt{3}$)$R30°$-K and Pt(111)-$c(2\times4)$-CO adsorption structures.

	Single adsorbates		Coadsorption		
	LEED	GGA	LEED	GGA	Change
	K/Pt(111)		K+CO/Pt(111)		
K adsorption cite	hcp	hcp	hcp	hcp	
K-Pt bondlength	3.16±0.03	3.16	3.28±0.06	3.26	+3.5 %
z_{12}	2.29±0.03	2.33	2.28±0.04	2.42	
	CO/Pt(111)		K+CO/Pt(111)		
CO adsorption cite	on-top/bridge	on-top/bridge	hcp	hcp	
C-O bondlength	1.12/1.19	1.14/1.17	1.26±0.06	1.27	+12 %
Pt-C bondlength	1.85/2.08	1.87/2.04	2.08±0.06	2.08	

For K+CO on Pt(111) the adsorption site of CO has been a subject for controversy in the past, both bridge and hollow sites or even geometries parallel to the surface have been postulated. The present LEED analysis determines the hcp site as the actual adsorption site. A comparison with the other coadsorption systems for which structural determinations exist suggests that a hollow site seems to be the favored site for CO in the presence of an alkali coadsorbate. For the (2×2) structures with K and Cs on Ru(0001) and with K on Ni(111) CO has also been found in hcp hollow sites; the alkali atom was, however, located on on-top sites in these slightly larger cells. In the Ru(0001) structures CO binds exclusively to the hcp site, in the Ni(111) structure CO is found in both hcp and fcc threefold hollow sites.

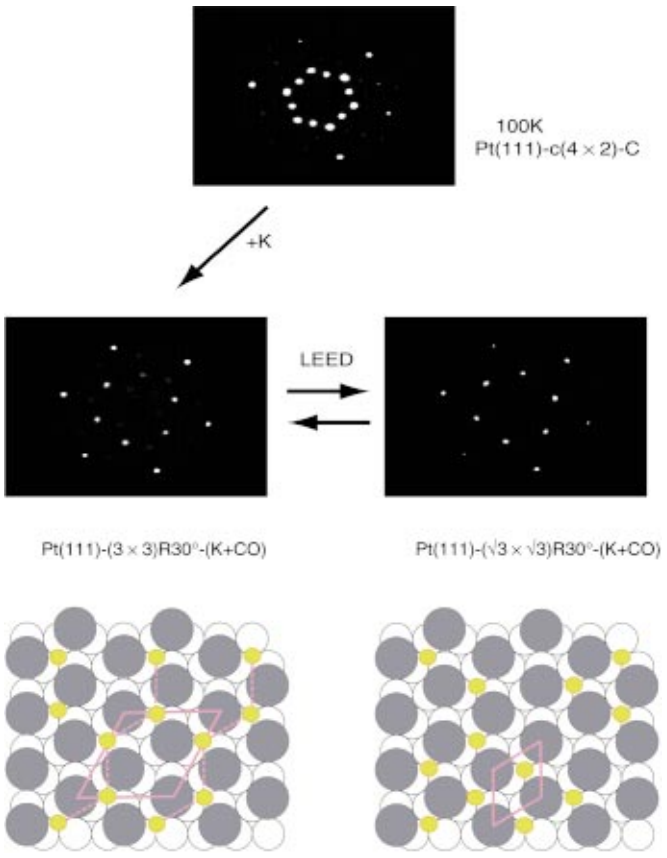

FIG. 4. (Color) LEED patterns observed during the formation of the ($\sqrt{3}\times\sqrt{3}$)$R30°$-(K+CO) structure with CO precoverage. The diagram bottom left shows a possible structure for the (3×3) phase.

Although alkali metal atoms adsorb in on-top sites in these (2×2) structures, there is a threefold coordination of the CO as observed for the structure presented in this paper. This would suggest that an important factor on surfaces with threefold or sixfold rotational symmetry is the mutual threefold coordination of the CO and the alkali adsorbate, the energy being lowest in the case when the CO occupies a hollow site.[8] So far all observed structures meet this criterion: the CO molecule on K/Pt(111), Cs/Ru(0001). CO on Ru(0001) and Co(0001) indeed shifts into hollow sites if an alkali metal is coadsorbed. On Ni(111) CO already occupies hcp and fcc sites in the pure CO phase. Due to the limited number of systems investigated so far we hesitate to draw any further conclusions at the present time.

The LEED and DFT-GGA analysis give very similar bondlengths for the adsorbates as shown in Table II. The structure is characterized by a relatively large increase in the C-O bondlength and a moderate increase in the K-Pt bondlength. The latter amounts to +0.12 Å or +3.5%. The corresponding values for K on CO/Ni(111), K on

TABLE III. r factors upon a variation of CO coverage for the best fit structure and CO precoverage. Bold values lie inside the error margins.

	$\theta=-5°$, $\theta=14°$		Normal incidence	
K:CO	R_{DE}	R_P	R_{DE}	R_P
1:0.5	**0.32**	**0.36**	0.39	0.45
1:1	0.37	**0.32**	0.39	**0.34**
1:1.25	0.38	0.40	**0.33**	**0.31**
1:1.5	0.42	0.62	0.45	0.46
1:2	0.82	0.83	0.53	0.73

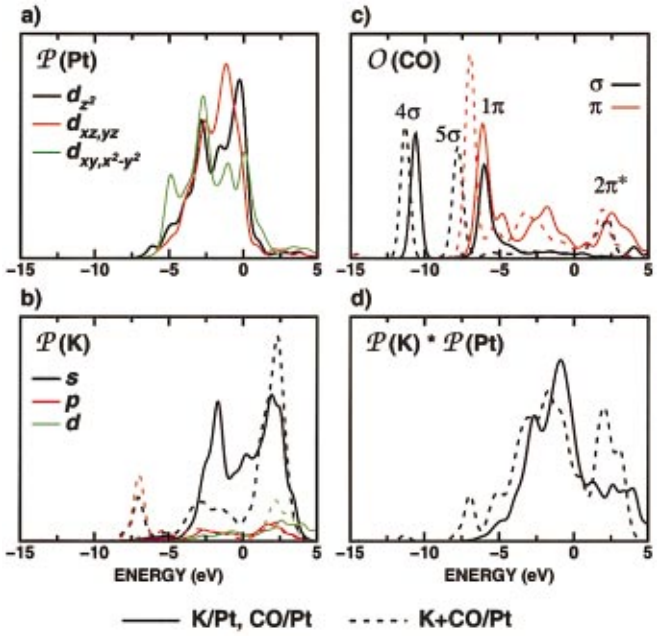

FIG. 5. (Color) Projected densities of states from the DFT-GGA calculation. (a) PDOS projected on the atomic *d* orbitals of a Pt atom on a clean Pt(111) surface. (b) PDOS projected on the atomic orbitals of a K atom. (c) Overlap of molecular CO orbitals with the states in the adsorption systems CO/Pt(111) and K+CO/Pt(111). (d) The product of the PDOS (summed over l,m) projected on the surface Pt and the adsorbed K atom. The solid lines in (b)–(d) are for a single adsorbate (K/Pt, CO/Pt) and the dashed line for the coadsorbed system (K+CO/Pt). The energies are given with respect to the Fermi energy of each individual system.

CO/Co($10\bar{1}0$), and Cs on CO/Ru(0001) are +0.4, +0.15, and +0.10 Å, respectively.[5] The increase in the K-substrate bondlength for the K+CO/Co($10\bar{1}0$) system is, however, partially due to the shift of the K towards a nonsymmetric site. The influence of the alkali adsorbate on the bondlength of the CO varies from system to system. The observed changes in bondlength are $+0.05\pm0.07$ Å for K/Ni(111), +0.11 Å for K/Ru(0001), and less than $+0.05\pm0.04$ Å for Cs/Ru(0001) depending on the CO coverage. These changes are smaller than for K/Pt(111).

The substantial lengthening of the C-O bond (1.26 versus 1.156 Å for the adsorbed CO and 1.13 Å for the free molecule) agrees well with the large shift in the C-O stretch frequency of 200–500 cm^{-1} as observed with EELS and IRAS.[7] The so-called Blyholder[37] mechanism, previously used to describe the bonding in metal carbonyl compounds and involving both donation of electrons from the σ orbitals of the CO and back donation into the CO $2\pi^*$ orbitals, is consistent with this result: The presence of the alkali metal atom increases the extent of backdonation and lowers the C-O stretching frequency. Wesner *et al.*[18] have suggested a formaldehydelike, double C-O bond configuration for CO coadsorbed with K on Pt(111).

Figure 5 depicts the energy resolved PDOS and orbital overlap of the orbitals involved in the K+CO coadsorption structure as resulting from the DFT-GGA calculation. Figure 5(a) shows the PDOS of the *d* orbitals of Pt atom at the clean surface. The *d* band ranges essentially from -6 to $+1$ eV relative to the Fermi energy. Figure 5(b) shows the projection of the Kohn-Sham states of K/Pt(111) (full lines) and K+CO/Pt(111) (dashed lines) onto the atomic orbitals of K. The potassium induces both an energy shift and an increase of the charge density over the whole energy range from -4 eV to above the Fermi energy, and this effect increases upon the coadsorption of CO to the K/Pt(111). The states above ≈ 2 eV might also be related to continuum states since the values of the work function, or ''ionization energy,'' for K/Pt(111) and K+CO/Pt(111) are 2.16 and 1.22 eV, respectively. With coadsorbed CO a peak appears at -7 eV relative to the Fermi energy which is due to an overlap of the K states with the molecular 5σ and 1π states of CO. That these orbitals influence the K PDOS might be an artifact due to the integration in the projection. However, due also to the short separation in the $(\sqrt{3}\times\sqrt{3})R30°$-(K+CO) structure this peak could also be regarded as an indication of a direct, covalent interaction between the coadsorbates.

Figure 5(c) shows the results of orbital overlap for CO at Pt(111) with and without the K coadsorbate. The large peak at about -11 eV below the Fermi energy without K arises mainly from the 4σ orbitals; the 5σ and 1π orbital energies are degenerate at -6 eV. The antibonding $2\pi^*$ lies about 2.5 eV above the Fermi energy, and one pronounced peak due to hybridization of the π orbitals with the substrate is situated around -2 eV. The coadsorption of K induces a downward shift of the orbital energies. Moreover, the degeneracy of the 5σ and 1π orbital energies is lifted: The 5σ orbital is pushed down to -8 eV, whereas the 1π, which is rather inactive towards external perturbations, is little affected. The unoccupied states are also pushed towards the Fermi energy, increasing somewhat the occupation of the $2\pi^*$ orbitals. The same downwards shift is visible in the product of $\mathcal{P}$(K)*$\mathcal{P}$(Pt) in Fig. 5(d); this could be interpreted as being due to a more positive, and thus for the electrons more attractive, potassium ion.

The new states which appear and the downward shift of the molecular CO-derived orbitals indicate a significant lengthening of the C-O bond. The elongation of the K-substrate bond might be seen in this context: An alkali metal atom, being an electron donor, increases the backbonding capabilities of the substrate. This charge transfer from the substrate to the adsorbate would require charge being donated by substrate orbitals of higher energy than the accepting adsorbate orbitals.

Another possibility which might explain both the elongated K-substrate bond and the elongated C-O bond would consist of a direct interaction between K and CO orbitals. Such an interaction and thus the resulting increase in the bondlengths would be more likely in the denser packed $(\sqrt{3}\times\sqrt{3})R30°$ structure than in the previously investigated (2×2) structures on Ru(0001) and Ni(111). The anisotropic vibration of the K atom found in the present LEED analysis provides some indication of this. The peak in Fig. 5(c) at -8 eV in the K+CO system could, as noted above, indicate an overlap of K and CO orbitals, an interaction which lengthens both the C-O bond and the K-substrate bond. This is in

agreement with the LEED result, which indeed shows an increase of the K-substrate distance as well as quantifies the C-O bond increase. A direct interaction between CO and K has been found to dominate the alkali promotor effect on Rh(111) by Liu and Hu[38] using DFT calculations. As the K-CO distance in our system is lower than the critical value of 3 Å (sum of the effective radii) it is likely that a certain degree of direct orbital interaction is present for the K/CO coadsorption system on Pt(111). This effect is, however, accompanied by a long-range effect as evident from the observation of the reversible self-ordering phase transition for structures prepared with a CO precoverage.

VI. CONCLUSIONS

K atoms in the $(\sqrt{3}\times\sqrt{3})R30°$-(K+CO) coadsorption phase on Pt(111) retain the hcp hollow site of the $(\sqrt{3}\times\sqrt{3})R30°$-K structure; the CO molecules also adsorb in hcp sites and are thus coordinated by three K atoms. If the structure is prepared starting from the Pt(111)-$c(2\times4)$-CO adsorption phase, CO molecules partially desorb and a (3×3) phase forms which is unstable under electron bombardment. The resulting $(\sqrt{3}\times\sqrt{3})R30°$-(K+CO) coadsorption phase exhibits the same structure as the structure that forms starting from the $(\sqrt{3}\times\sqrt{3})R30°$-K-adsorption phase. The geometrical parameters determined independently with LEED structure analysis and DFT-GGA calculations are in good agreement. Both the K-Pt and C-O bondlengths are increased due to the coadsorption relative to those in the pure phases on the same surface.

ACKNOWLEDGMENTS

We would like to thank Dr. P. Kratzer for useful discussions regarding the interpretation of the DFT-GGA results. We are greatly indebted to W. Moritz for allowing us to use his program and for supplying the platinum phase shifts as well as to M. Gierer and H. Over for valuable discussions. The work was supported by the Deutsche Forschungsgemeinschaft within the Sonderforschungsbereich 290.

*Present address: UVSOR, Institute for Molecular Science, Myodaiji, Okazaki, Aichi 444-8585, Japan; electronic address: more@ims.ac.jp

†Email address: Ari.P.Seitsonen@iki.fi; URL: http://www.iki.fi/~apsi/

[1] G. Ertl, in *The Physics and Chemistry of Alkali Metal Adsorption*, edited by H. P. Bonzel, A.M. Bradshaw, and G. Ertl (Elsevier, Amsterdam, 1989).

[2] J.E. Crowell, E.L. Garfunkel, and G.A. Somorjai, Surf. Sci. **121**, 303 (1982).

[3] H.P. Bonzel, Surf. Sci. Rep. **8**, 43 (1987).

[4] D. Heskett, Surf. Sci. **199**, 67 (1988).

[5] R. Diehl and R. Mc Grath, Surf. Sci. Rep. **23**, 43 (1996).

[6] L. Wallden, Surf. Sci. **134**, L513 (1983); V. Dose, J. Ragozik, A.M. Bradshaw, and K.C. Prince, *ibid.* **179**, 90 (1987).

[7] M. Tüshaus, P. Gardner, and A.M. Bradshaw, Surf. Sci. **286**, 212 (1993).

[8] H. Over, Prog. Surf. Sci. **58**, 249 (1998).

[9] H. Over (private communication).

[10] H. Over, H. Bludau, R. Rose, and G. Ertl, Surf. Sci. **331-333**, 323 (1995).

[11] P. Kaukasoina, M. Lindroos, P. Hu, D.A. King, and C.J. Barnes, Phys. Rev. B **51**, 17 063 (1995).

[12] R. Davis, D.P. Woodruff, O. Schaff, V. Fernandez, K. M. Schindler, P. Hofmann, K.U. Weiss, R. Dippel, V. Fritzsche, and A.M. Bradshaw, Phys. Rev. Lett. **74**, 1621 (1995).

[13] C. Stampfl, M. Scheffler, H. Over, J. Burchhardt, M. Nielsen, D.L. Adams, and W. Moritz, Phys. Rev. Lett. **69**, 1532 (1992).

[14] S. Moré, W. Berndt, A.M. Bradshaw, and R. Stumpf, Phys. Rev. B **57**, 9246 (1998).

[15] S. Moré, Ari P Seitsonen, W. Berndt, and A.M. Bradshaw, Phys. Rev. B **63**, 075406 (2001).

[16] G. Pirug and H.P. Bonzel, Surf. Sci. **199**, 371 (1988).

[17] E.L. Garfunkel, J.E. Crowell, and G.A. Somorjai, J. Phys. Chem. **86**, 310 (1992).

[18] D. A. Wesner, G. Pirug, F.P. Coenen, and H.P. Bonzel, Surf. Sci. **178**, 608 (1986).

[19] J. Müller, in *Coadsorption, Promoters and Poisons*, Vol. 6 of *The Chemical Physics on Solid Surfaces*, edited by D.A. King and D.P. Woodruff (Elsevier, Amsterdam, 1993).

[20] J.J. Weimer, E. Umbach, and D. Menzel, Surf. Sci. **155**, 132 (1985).

[21] D.F. Ogletree, M.A. van Hove, and G.A. Somorjai, Surf. Sci. **183**, 1 (1987).

[22] W. Moritz, J. Phys. C **17**, 353 (1988).

[23] J.B. Pendry, *Low Energy Electron Diffraction* (Academic Press, London, 1971).

[24] V.L. Moruzzi, J.F. Janak, and A.R. Williams, *Calculation of Electronic Properties of Metals* (Plenum, New York, 1978).

[25] J.B. Pendry, J. Phys. C **13**, 937 (1980).

[26] G. Kleinle, W. Moritz, and G. Ertl, Surf. Sci. **238**, 119 (1990).

[27] S. Schwegmann and H. Over, Surf. Sci. **360**, 271 (1996).

[28] H. Over, H. Bludau, M. Skottke-Klein, G. Ertl, W. Moritz, and C.T. Campbell, Phys. Rev. B **45**, 8638 (1992); M. Gierer, H. Bludau, T. Hertel, H. Over, W. Moritz, and G. Ertl, Surf. Sci. **279**, L170 (1992); T. Hertel, H. Over, H. Bludau, M. Gierer, and G. Ertl, *ibid.* **279**, 8126 (1994).

[29] M. Caragiu, G.S. Leatherman, R.D. Diehl, P. Kaukasoina, and M. Lindroos, Surf. Sci. **441**, 84 (1999).

[30] S. Moré, Ph.D. thesis, Freie Universität Berlin, 1998.

[31] J.P. Perdew, in *Electronic Structure of Solids '91*, edited by P. Ziesche and H. Eschrig (Akademie Verlag, Berlin, 1991); J.P. Perdew, J.A. Chevary, S.H. Vosko, K.A. Jackson, M.R. Pederson, D. J. Singh, and C. Fiolhais, Phys. Rev. B **46**, 6671 (1992); John P. Perdew, Kieron Burke, and Yue Wang, *ibid.* **54**, 16 533 (1996).

[32] Specifically the Troullier-Martins pseudopotentials [N. Troullier and J. L. Martins, Phys. Rev. B **43**, 1993 (1991)]; Martin Fuchs (private communication)] were generated, and the $4s$, $4p$, and $3d$ orbitals as the valence states in the pseudopotential for potassium due to the energetically high semicore states; additionally we applied the nonlinear core-valence exchange-correlation scheme [S.G. Louie, S. Froyen, and M. L. Cohen, Phys. Rev. B **26**, 1738 (1982)] with a radius $r_{\mathrm{NLCV,K}}=0.8$ Bohr. We used cut-

off radii $r_c^{l=s}=2.4$, $r_c^{l=p}=2.5$, and $r_c^{l=d}=2.2$ Bohr for the platinium, $r_c^{l=s,d}=1.45$ and $r_c^{l=p}=1.40$ Bohr for the potassium, $r_c^{l=s}=1.25$ and $r_c^{l=p,d}=1.2$ Bohr for carbon, and $r_c^{l=s,d}=1.25$ and $r_c^{l=p}=1.4$ Bohr for oxygen. The *s*, *p*, *d*, and *d* potentials were used as the local components for the pseudopotential, respectively.

[33] J. Neugebauer and M. Scheffler, Phys. Rev. B **46**, 16 067 (1992); Lennart Bengtsson, *ibid.* **59**, 12 301 (1999).

[34] S.L. Cunningham, Phys. Rev. B **10**, 4988 (1974); A. P Seitsonen, in preparation and Ref. 35.

[35] Ari P Seitsonen, Ph.D. Thesis, TU Berlin, 2000; URL http://www.iki.fi/~apsi/Thesis.html

[36] A. P Seitsonen (unpublished).

[37] G. Blyholder, J. Phys. Chem. **68**, 2772 (1964).

[38] Z.P. Lui and P. Hu, J. Am. Chem. Soc. **123**, 12596 (2001).